Earthquakes and Structures, *Vol. 15, No. 5 (2018) 463-471*
DOI: https://doi.org/10.12989/eas.2018.15.5.463

Damage detection of a thin plate using pseudo local flexibility method

Ting Yu Hsu* and Chao Lun Liu[a]

Department of Civil and Construction Engineering, National Taiwan University of Science and Technology, Taipei, Taiwan

(Received May 20, 2017, Revised June 12, 2018, Accepted August 28, 2018)

Abstract. The virtual forces of the original local flexibility method are restricted to inducing stress on the local parts of a structure. To circumvent this restriction, we developed a pseudo local flexibility (PLFM) method that can successfully detect damage to hyperstatic beam structures using fewer modes. For this study, we further developed the PLFM so that it could detect damage in plate structures. We also devised the theoretical background for the PLFM with non-local virtual forces for plate structures, and both the lateral and rotary degree of freedom (DOF) measurements were considered separately. This study investigates the effects of the number of modes, the actual location that sustained damage, multiple damage locations, and noise in modal parameters for the damage detection results obtained from damaged numerical plates. The results revealed that the PLFM can be used for damage detection, localization, and quantification for plate structures, regardless of the use of the lateral DOF and/or rotary DOF.

Keywords: pseudo local flexibility method; rotary DOF; long gauge; plate; damage detection

1. Introduction

Plate structures are widely used as important structural components in many engineering fields, including civil, mechanical, aerospace, and automotive engineering. Structural condition assessments of in-service plate structures play a critical role in global structural health monitoring. In recent years, the research community has paid particular attention to vibration-based structural damage detection techniques that can be used to perform damage diagnosis based on modal parameters (e.g., Doebling *et al*. 1996, Salawu 1997, Caicedo 2003, Giraldo 2006).

Among studies on vibration-based structural damage detection methods, those that focus on their application to 2D plate-type structures are relatively limited. Cawley and Adams (1979) were probably the first to detect damage on a rectangular plate using frequency shifts. Many other methods for detecting damage in plate-like structures have also been proposed based on finite element models (e.g., Dos Santos *et al*. 2005, Ge and Lui 2005, Fu *et al.* 2013).

However, a number of proposed vibration-based methods are capable of detecting damage to plate-like structures without requiring any information from a finite element model. For instance, to locate the damaged area of a plate, Cornwell *et al*. (1999) used a damage index based on the fractional strain energy calculated from measured mode shapes with many points. Moreover, Bayissa and Haritos (2007) proposed using the spectral strain energy derived from a moment-curvature response to detect damage to a plate-like structure. Thus, damage locations can be identified using non-mass-normalized mode shapes and natural frequencies, without requiring a finite element model.

Fan and Qiao (2009) applied a 2D continuous wavelet transform algorithm on mode shapes with dense grids that were identified with a roving excitation test. They compared the proposed algorithm against the 2D gapped smoothing method and the 2D strain energy method, and concluded that the proposed method outperformed its counterparts. Zhang *et al*. (2013) applied a modal-frequency-based method to a steel plate by using the 2D gapped smoothing method to calculate the residual values. To detect and localize damage in plate-like structures through vibration testing, the method employs variations of modal frequency data as a roving mass traverses to various locations on a plate.

Ng (2015) proposed using a dual-stage imaging approach for quantitative damage inspection in metallic plates by using the fundamental antisymmetric mode of the Lamb wave. He employed a number of transducers to transmit and receive Lamb wave pulses, thereby sequentially scanning the plate structures before and after the occurrence of damage. Torkzadeh *et al*. (2016) proposed a novel two-stage methodology for damage detection to flexural plates by using an optimized artificial neural network. Their study investigated the location of damaged areas in the plates by using curvature-moment and curvature-moment derivative concepts in the first stage. Afterward, using a properly trained cascade feed-forward neural network as a surrogate model, they evaluated an index of the multiple-damage location assurance criterion based on the frequency change vector of the structures.

Reynders and De Roeck (2010) recently developed the local flexibility method (LFM); its theoretical foundations

*Corresponding author, Assistant Professor
E-mail: tyhsu@mail.ntust.edu.tw
[a]Graduate Student
E-mail: m10505331@mail.ntust.edu.tw

ISSN: 2092-7614 (Print), 2092-7622 (Online)

are robust, and the method can be used to determine not only the damage location but also the extent of damage sustained. The general procedure of the LFM involves using flexibility matrices and designated virtual forces that generate locally restricted stress fields in the structure to perform damage localization and quantification.

The structural modal parameters identified from the ambient vibration signals both before and after damage can be used to construct the flexibility matrices, and are key data for the LFM. Thus, the LFM does not require a finite element model of the structure. The general theory of the LFM has been applied to beam structures for damage detection, and few modes are typically necessary.

Especially for simple cases such as those involving a simply supported beam, there are conditions where the first mode alone suffices. However, for a hyperstatic beam or other, more complex structures, the number of modes required for damage estimation can increase significantly. This reduces the feasibility of the LFM because, in practice, only the first few modes can be identified accurately using ambient vibration signals.

Moreover, application of the LFM to other structures has not been achieved, mainly because of the difficulty in identifying virtual forces guaranteed to limit the existence of the induced stress to the local region of another structure (e.g., a plate structure).

Hsu *et al*. (2014) developed the pseudo local flexibility method (PLFM), which successfully detects damage to hyperstatic beam structures using fewer modes. The PLFM eliminates the limitation of virtual forces inducing stress only to the local part of a structure, as is the case with the LFM.

In this manner, the non-local virtual forces that generate concentrated stresses in a local part, and relatively small stresses in other parts of a structure, can be employed. Most importantly, removing this limitation enables the identification of suitable virtual forces for plate structures.

Therefore, this study proposes employing the PLFM for damage detection in plate structures. First, we lay out the theoretical basis for the PLFM (using non-local virtual forces for plate structures). We then investigate the effects of the number of modes, the damage location, multiple damage locations, and the noise in the modal parameters on the damage detection results for the numerical plates. Both lateral and rotational degree of freedom (DOF) measurements are considered separately. The results indicate that both the damage locations and the extent of the damage sustained can be estimated using a few modal parameters identified from the measured vibration signals.

2. Pseudo local flexibility method for thin plates

The PLFM considers a structure with volume, Ω, and boundary, Γ, that is subjected to Dirichlet boundary conditions along a part of the boundary. A first load configuration, f^1, is applied at a limited number of r DOFs, where the response can be measured. The first load configuration for the PLFM is chosen such that the induced stress field, σ^1, consists of concentrated stresses in the local volume, Ω_p, and a small stress outside Ω_p (i.e., Ω_q), as

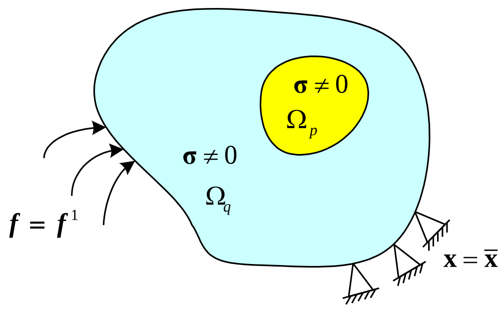

Fig. 1 Structure subjected to the first load configuration, f^1, causing concentrated stress within the local region Ω_p, and relatively small stress outside the local region

shown in Fig. 1. The first load configuration f^1 is assumed to only cause non-zero stress within Ω_p for the LFM. Based on the virtual work principle with the body force neglected

$$\int_{\Gamma} t^T \delta x d\Gamma = \int_{\Omega} \sigma^T \delta\varepsilon d\Omega \tag{1}$$

where t is the vector with applied tractions, σ represents the corresponding stress vector, δx is a virtual displacement field that obeys the Dirichlet boundary conditions, and $\delta\varepsilon$ depicts the corresponding virtual strain vector. If the virtual displacement field is chosen as that induced by f^1, but the forces and stresses are due to the second load configuration, f^2, which obeys the boundary conditions of the system, then we derive the following

$$\sum_{j=1}^{r} f_j^2 x_j^1 = \int_{\Omega_p} (\sigma_p{}^2)^T \varepsilon_p{}^1 d\Omega_p + \int_{\Omega_q} (\sigma_q{}^2)^T \varepsilon_q{}^1 d\Omega_q \tag{2}$$

where x_j^1 is the displacement at DOF j corresponding to f^1. Assume that the structure is linearly elastic, and that σ^1 is proportional to ε^1, with stiffness constant K. If the virtual work is calculated both before and after the damage has occurred, we obtain the following

$$\frac{\sum_{j=1}^{r} f_j^2 x_j^1}{\sum_{j=1}^{r} f_j^2 x_{jd}^1} = \frac{\int_{\Omega_p} (\sigma_p{}^2)^T \frac{\sigma_p{}^1}{K_p} d\Omega_p + \int_{\Omega_q} (\sigma_q{}^2)^T \frac{\sigma_q{}^1}{K_q} d\Omega_q}{\int_{\Omega_p} (\sigma_{pd}{}^2)^T \frac{\sigma_{pd}{}^1}{K_p+\Delta K_p} d\Omega_p + \int_{\Omega_q} (\sigma_{qd}{}^2)^T \frac{\sigma_{qd}{}^1}{K_q+\Delta K_q} d\Omega_q} \tag{3}$$

where subscript d represents the parameter of the structure in a damaged state. Assume that stresses σ^1 and σ^2 are concentrated within the local volume Ω_p, and σ^1 and σ^2 outside the local volume are small; hence, the strain energy outside the local volume is much smaller than that within the local volume. We can neglect the strain energy outside the local volume, and obtain

$$\frac{\sum_{j=1}^{r} f_j^2 x_j^1}{\sum_{j=1}^{r} f_j^2 x_{jd}^1} \cong \frac{\int_{\Omega_p} (\sigma_p{}^2)^T \frac{\sigma_p{}^1}{K_p} d\Omega_p}{\int_{\Omega_p} (\sigma_{pd}{}^2)^T \frac{\sigma_{pd}{}^1}{K_p+\Delta K_p} d\Omega_p} \tag{4}$$

Assume that K and ΔK are constant within Ω_p, which means that only the lump estimation of K and ΔK within Ω_p can be achieved. They can then be moved outside the integration, to obtain

$$\frac{\sum_{j=1}^{r} f_j^2 x_j^1}{\sum_{j=1}^{r} f_j^2 x_{jd}^1} \cong \frac{\frac{1}{K_p}\int_{\Omega_p} ({\sigma_p}^2)^T {\sigma_p}^1 d\Omega_p}{\frac{1}{K_p+\Delta K_p}\int_{\Omega_p} ({\sigma_{pd}}^2)^T {\sigma_{pd}}^1 d\Omega_p} \tag{5}$$

Further, we assume that the stress does not change significantly once the plate sustains damage; therefore, the integration of both the numerator and the denominator are similar, and cancel each other out. Eq. (5) thus becomes

$$\frac{\sum_{j=1}^{r} f_j^2 x_j^1}{\sum_{j=1}^{r} f_j^2 x_{jd}^1} \cong \frac{K_p + \Delta K_p}{K_p} \tag{6}$$

Although this general theory is applicable to many elastic structures, in this study, we applied the theory only to thin-plate structures. For an isotropic quasistatic Kirchhoff-Love plate (Timoshenko 1959), the stress-strain relations are expressed as follows

$$\begin{bmatrix}\sigma_{xx}\\ \sigma_{yy}\\ \sigma_{xy}\end{bmatrix} = \frac{E}{1-\nu^2}\begin{bmatrix}1 & \nu & 0\\ \nu & 1 & 0\\ 0 & 0 & 1-\nu\end{bmatrix}\begin{bmatrix}\epsilon_{xx}\\ \epsilon_{yy}\\ \epsilon_{xy}\end{bmatrix} \tag{7}$$

The moment M_{xx} can be derived as

$$M_{xx} = \int_{-h/2}^{h/2} z\sigma_{xx} dz = \int_{-h/2}^{h/2} \frac{E}{1-\upsilon^2}(\epsilon_{xx} + \nu\epsilon_{yy})zdz \tag{8}$$

where $\frac{Eh^3}{12(1-\nu^2)}$ is typically denoted as D, the flexural rigidity in plate theory, and h is the thickness of the plate. Because $K_{xx} = -\frac{\partial^2 w}{\partial x^2}$ and $K_{yy} = -\frac{\partial^2 w}{\partial y^2}$, (8) can be simplified as

$$M_{xx} = D(K_{xx} + \nu K_{yy}) \tag{9}$$

In a similar manner, M_{xy} and M_{yy} can be obtained with

$$M_{yy} = D(\nu K_{xx} + K_{yy}) \tag{10}$$

$$M_{xy} = (1-\nu)DK_{xy} \tag{11}$$

From (9) to (11), we can derive the curvatures K_{xx}, K_{yy}, and K_{xy}, as follows

$$\begin{aligned} K_{xx} &= \frac{1}{D(1-\nu^2)}(M_{xx} - \nu M_{yy}) \\ K_{yy} &= \frac{1}{D(1-\nu^2)}(M_{yy} - \nu M_{xx}) \\ K_{xy} &= \frac{M_{xy}}{D(1-\nu^2)} \end{aligned} \tag{12}$$

If the shear strain energy is small enough to be negligible, the strain energy of the plates can be derived using (12)

$$\begin{aligned} U = \iint & M_{XX}\left[\frac{1}{D(1-\nu^2)}(M_{xx} - \nu M_{yy})\right] \\ &+ M_{yy}\left[\frac{1}{D(1-\nu^2)}(M_{yy} - \nu M_{xx})\right] \\ &+ 2M_{xy}\left[\frac{M_{xy}}{D(1-\nu^2)}\right] dxdy \end{aligned} \tag{13}$$

If D and Poisson's ratio are constant, the strain energy can be derived as follows

$$\begin{aligned} U &= \frac{1}{D(1-\nu^2)}\iint M_{XX}(M_{xx} - \nu M_{yy}) \\ &\quad + M_{yy}(M_{yy} - \nu M_{xx}) + 2{M_{xy}}^2 dxdy \end{aligned} \tag{14}$$

$$= \frac{12}{Eh^3}\iint {M_{XX}}^2 + 2\nu M_{XX}M_{yy} + {M_{yy}}^2 + 2{M_{xy}}^2 dxdy$$

If we denote $s = Eh^3/12$, which represents the flexural rigidity of a unit width of the plate structure, then

$$U = \frac{1}{S}\iint {M_{XX}}^2 + 2\nu M_{XX}M_{yy} + {M_{yy}}^2 + 2{M_{xy}}^2 dxdy \tag{15}$$

Because the virtual strain energy of a plate structure can be represented with this equation, following the process from (1) to (6), based on the PLFM concept, the damage detection equation for the isotropic quasistatic Kirchhoff-Love plate can be derived as

$$\frac{\sum_{j=1}^{l} f_j^2 x_j^1}{\sum_{j=1}^{l} f_j^2 x_{jd}^1} \cong \frac{(\mathrm{S}_p + \Delta \mathrm{S}_p)}{\mathrm{S}_p} \equiv \mathrm{R} \tag{16}$$

where R represents the lumped rigidity ratio of the local region of a plate structure.

The virtual displacement vector, x^1, under f^1, can be obtained with

$$x^1 = Hf^1 \tag{17}$$

where H represents the flexibility matrix. The flexibility matrix H can be obtained directly from a static load-deflection test, or by conducting a forced vibration test. Under the assumption of a lumped and approximately equal mass distribution, the flexibility matrix can also be estimated using the identified modal parameters, as follows (Reynders and De Roeck 2010)

$$H \cong H^n = -\Phi{\Lambda_c}^{-1}({\Lambda_c}^H\Phi^H\Phi\Lambda_c + \Phi^H\Phi)^{-1}{\Lambda_c}^H\Phi^H \tag{18}$$

where Φ is the matrix of the mode shapes, Λ_c represents the diagonal matrix of the system poles, and ^{H} is the Hermitian transpose. If only the first n modes are available, then the flexibility matrix is truncated, and denoted as H^n.

In this study, all the flexibility matrices were estimated using (18). Contrary to the stiffness matrix, the contribution of the modes in the flexibility matrix are proportional to the inverse of the square of the system poles. The higher modes on the flexibility matrix have a much smaller influence compared to the lower modes. Consequently, fewer truncated modes are required to approximate a non-truncated flexibility matrix than to approximate a non-truncated stiffness matrix. This benefits practical cases where only a limited number of lower modes can be identified with an acceptable level of accuracy, a situation that is prevalent when using ambient vibration signals.

The first virtual force, f^1, for the proposed PLFM was assumed to cause only concentrated stress within Ω_p. For plate structures, if the transverse DOFs are being measured, the virtual force configuration displayed in Fig. 2 is a good option because it is simple and symmetric. However, if the rotational DOFs are being measured, then the virtual force configuration consists of the moment, and could be even simpler (Fig. 3).

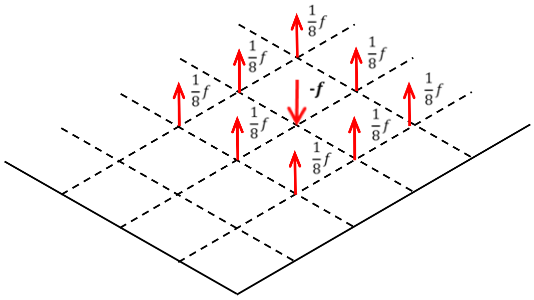

Fig. 2 Potential virtual force configuration for a thin-plate structure if the lateral DOFs are measured

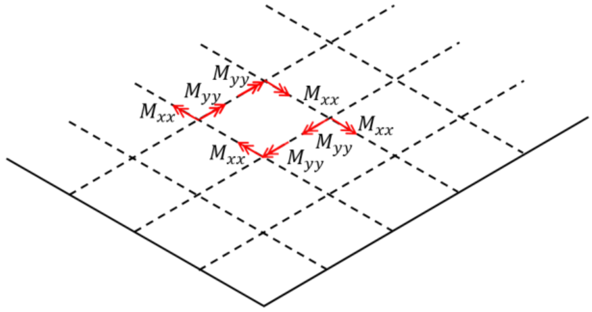

Fig. 3 Potential virtual force configuration for a thin-plate structure if the rotational DOFs are measured

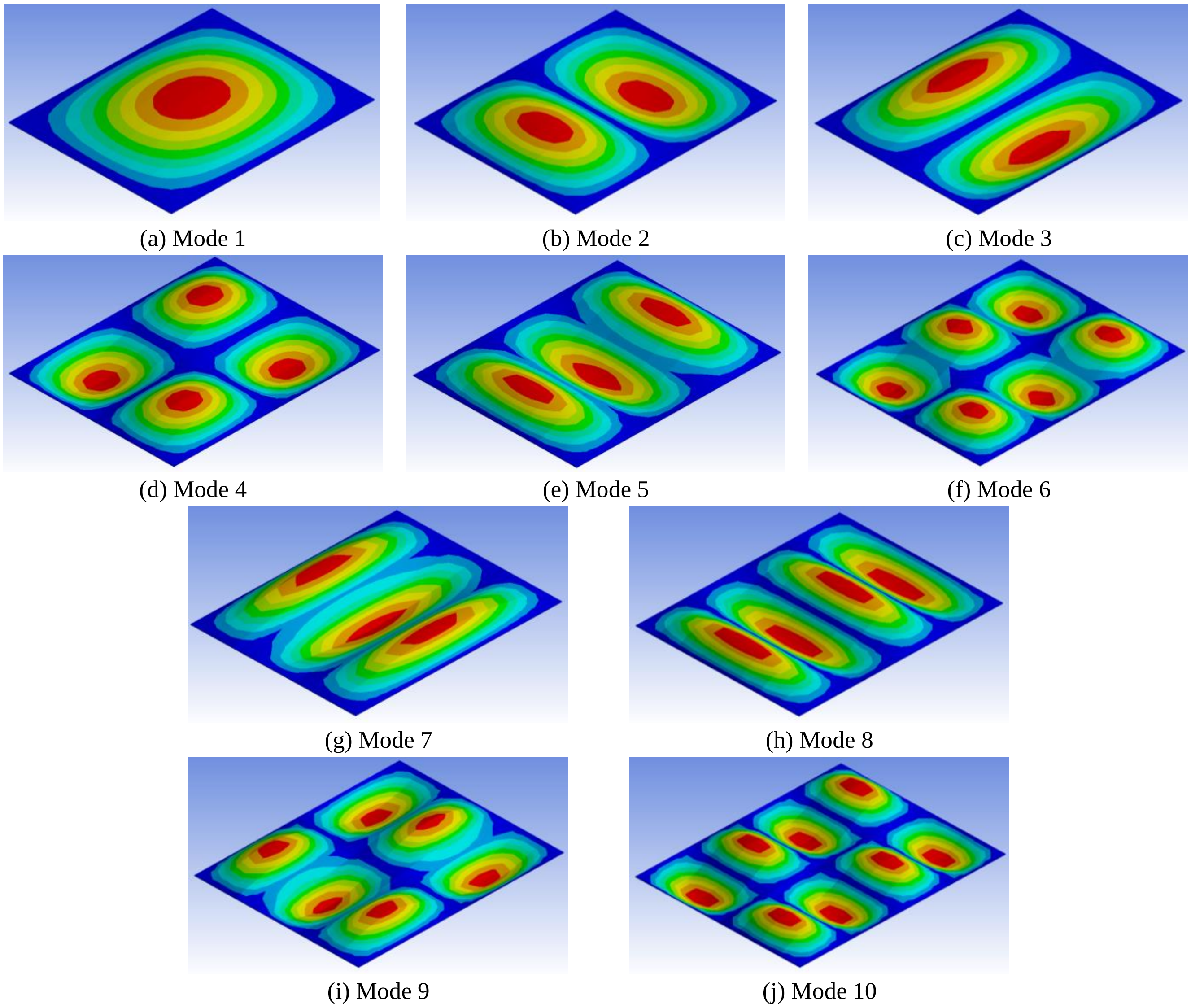

(a) Mode 1 (b) Mode 2 (c) Mode 3

(d) Mode 4 (e) Mode 5 (f) Mode 6

(g) Mode 7 (h) Mode 8

(i) Mode 9 (j) Mode 10

Fig. 4 The first 10 mode shapes of the plate structure

The calculation of the PLFM includes the use of the identified modal parameters to construct the truncated flexibility matrix with (18); afterward, the truncated flexibility matrix is multiplied by the first load configuration to obtain the virtual displacement, as shown in (17); finally, the virtual displacement is multiplied by the second load configuration both before and after the occurrence of damage, as shown in (16). The first and second virtual load configurations can be identical, and were used in this study.

3. Numerical studies

For this study, we constructed a thin-plate model using ANSYS software to verify the proposed approach. The

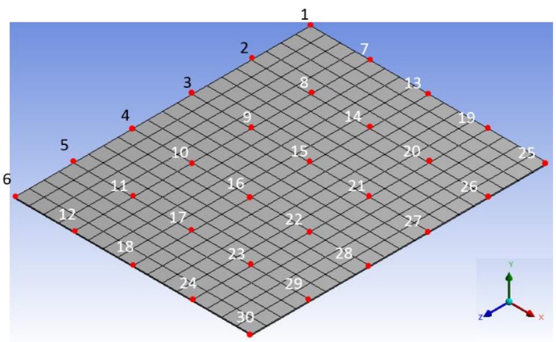

Fig. 5 Thirty points of the numerical model with vertical and rotational response measurements

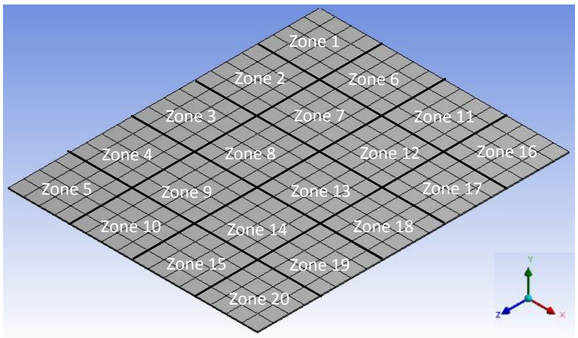

Fig. 6 Twenty zones for estimating the rigidity ratios of the plate structure by using the virtual force configuration shown in Fig. 2

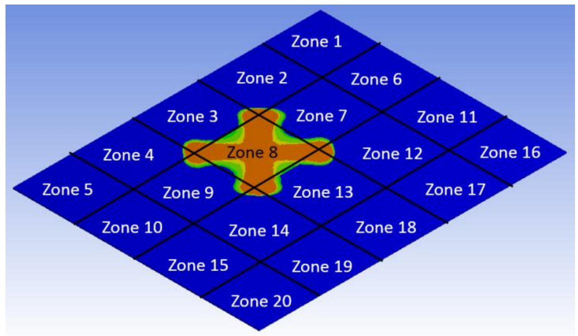

Fig. 7 Equivalent tensile stress distribution of the plate induced by the virtual force configuration shown in Fig. 3 around Zone 8

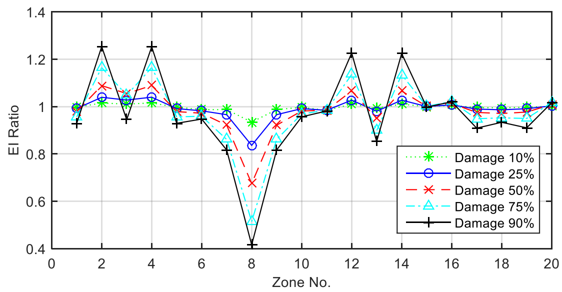

Fig. 8 Rigidity ratio of the plate structure estimated using the first 10 modes when the elastic modulus of Zone 8 was reduced to 10%, 25%, 50%, 75%, and 90% using rotational DOF mode shapes

plate dimensions were 1500 mm×1200 mm×5 mm, and the shell elements along the two edges both measured 5 mm during soft mesh sizing. The elastic modulus, Poisson's ratio, and the density of the finite element model were 2.0×10^{11} N/m^2, 0.33, and 7.8×10^3 kg/m^3, respectively. The plate was supported by hinges along the four boundaries, resulting in a first fundamental frequency of 1 Hz. The first 10 mode shapes are displayed in Fig. 4. The vertical and rotational responses were measured at 30 points (Fig. 5).

Four damage scenarios were considered for this study: 1) Varying the extent of damage. The elastic modulus of the eighth region was reduced to 10%, 25%, 50%, 75%, and 90%; 2) Varying the location of damage. Considering the symmetry of the plate, the elastic moduli of the first, second, third, sixth, seventh, and eighth regions were reduced to 50%. We also studied the effect on the damage detection results obtained by varying the numbers of modes; 3) Damage to both the first and eighth regions with a 50% reduction in elastic modulus to simulate multiple damage locations; and 4) The effect of the measurement noise by adding a normal distributed error with a 2% standard deviation in the modal parameters when the elastic modulus of the eighth region was reduced to 50%.

3.1 PLFM using rotational DOFs

First, we used the rotational DOFs of the mode shapes to construct the flexibility matrices; hence, the corresponding virtual moments were employed. The force configuration shown in Fig. 3 was applied as both f^1 and f^2. The plate was divided into 20 zones, according to the measurement setup and virtual force configuration shown in Fig. 6. For example, if the force configuration displayed in Fig. 3 was applied at Points 9, 10, 15, and 16, the estimated results were chiefly representative of the rigidity ratio within the eighth zone.

The equivalent tensile stress distribution of the plate induced by the virtual force configuration applied at this set of points is shown in Fig. 7. We observed that stress was concentrated within the eighth zone; hence, based on the theoretical basis of the PLFM, the rigidity ratio of the eighth zone could be estimated. By applying the virtual force configuration at different sets of points, the rigidity ratio within each of the 20 zones could be estimated. The corresponding displacements, x^1, for each of the measured DOFs could thus be calculated using the truncated flexibility matrices constructed with a different number of modes and f^1 by solving for (18).

Fig. 8 shows the estimated rigidity ratio, *R*, when the elastic modulus of Zone 8 was reduced to 10%, 25%, 50%, 75%, and 90% using the first 10 modes. The location of the damage could be identified clearly with the estimated *R* using the PLFM with rotational DOF mode shapes. However, the extent of damage in Zone 8 was somewhat underestimated for all five levels of damage.

Fig. 9(f) shows *R* when the elastic modulus of Zone 8 was reduced to 50% using the first one, three, five, seven, and ten modes. The results evidently improved as more modes were used. Even the results obtained using only the first mode already indicated the damage location clearly,

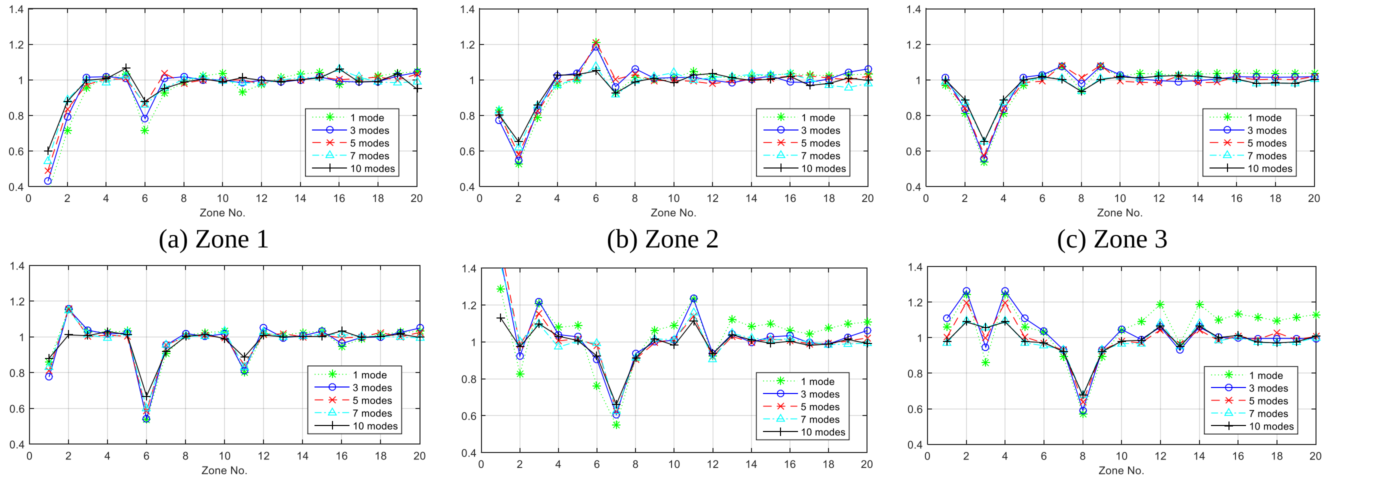

(a) Zone 1 (b) Zone 2 (c) Zone 3

(d) Zone 6 (e) Zone 7 (f) Zone 8

Fig. 9 Rigidity ratios estimated using the first one, three, five, seven, and ten modes when the elastic modulus of (a) Zone 1, (b) Zone 2, (c) Zone 3, (d) Zone 6, (e) Zone 7, and (f) Zone 8 was reduced to 50% using rotational DOF mode shapes

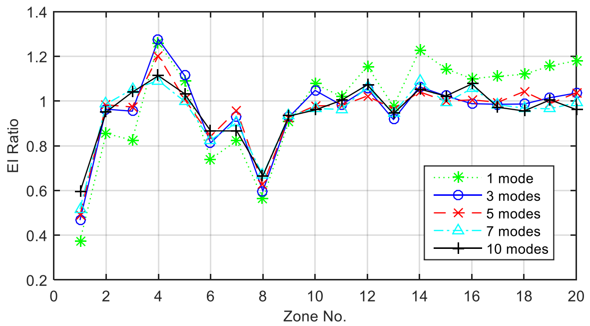

Fig. 10 Rigidity ratio estimated when both Zones 1 and 8 were damaged, with a 50% reduction in elastic modulus using rotational DOF mode shapes

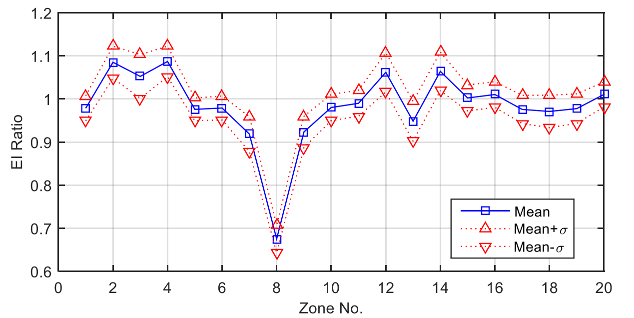

Fig. 11 Estimated rigidity ratio with 2% random noise in modal parameters when the elastic modulus of Zone 8 was reduced by 50% using rotational DOF mode shapes

and the estimated extent of damage to Zone 8 was quite close to that found using the first 10 modes.

Another noteworthy finding is that the estimated rigidity ratios of the zones adjacent to the damaged eighth zone (i.e., Zones 3, 7, 9, and 13) were somewhat affected by the damaged zone. This could be due to the non-zero stress within the damaged zone when the virtual force configuration was applied to these adjacent zones. Hence, the virtual work within the adjacent zones before and after sustaining damage also changed due to the nearby damaged zone. When different zones were subjected to the same extent of damage, and the same number of modes were used, we observed a similar phenomenon to that shown in the images in Fig. 9.

When both Zones 1 and 8 were damaged with a 50% reduction in elastic modulus, the results shown in Fig. 10 were obtained using the first 10 modes. Clearly, both damage zones were identified, and even the results obtained using only the first mode already identified the damage locations and severity with an acceptable level of accuracy.

The estimated rigidity ratio was relatively similar to that obtained when only one zone was damaged to the same extent. In other words, the damage detection results for the two damage locations were similar to those obtained if both the damage results of the individual damage locations were simultaneously considered. This phenomenon implies that the damage detection results may not be seriously affected by multiple damage locations.

In the final scenario, both the modal frequencies and mode shapes of the first 10 modes were contaminated with 2% random noise, within one standard deviation. The damage results obtained when the elastic modulus of Zone 8 was reduced by 50% are shown in Fig. 11. We conducted 100 trials and calculated the mean value as well as the mean value plus or minus one standard deviation of the rigidity ratios. The maximum and minimum of the standard deviation of all the estimated rigidity ratios in the different zones were 4.54% and 2.90%, respectively. The amount of the standard deviation is acceptable compared to the estimated reduction in the rigidity ratio, which was approximately 33%.

3.2 PLFM using lateral DOFs

In most cases, the lateral acceleration vibration records are measured for plate-like structures. Therefore, the lateral DOF mode shapes are also considered, and can be used to construct the flexibility matrices to estimate the rigidity ratio.

The force configuration shown in Fig. 2 was applied as

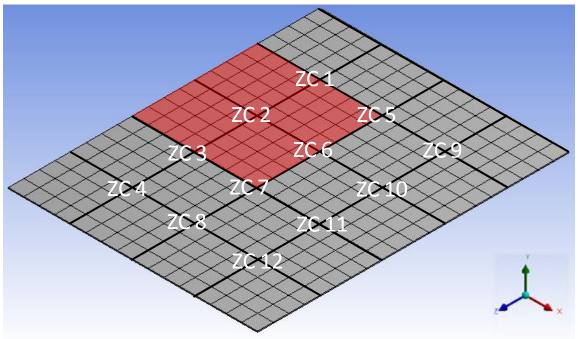

Fig. 12 Twelve zone combinations for estimating the rigidity ratios of the plate structure using the virtual force configuration shown in Fig. 3

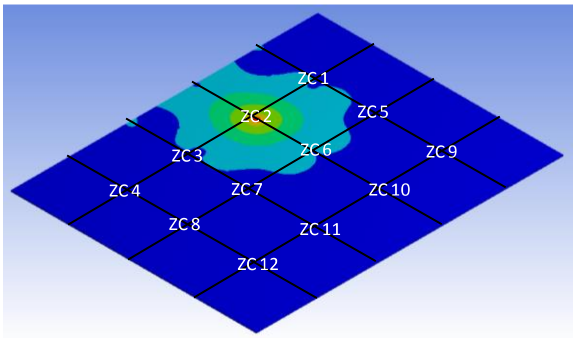

Fig. 13 Equivalent tensile stress distribution of the plate induced by the virtual force configuration shown in Fig. 3 around the second zone combination

both f^1 and f^2. According to the measurement setup and virtual force configuration, we can estimate the average rigidity ratio of 12 zone combinations (ZC) of the mentioned 20 zones (Fig. 12). For example, if the force configuration were to be applied at Points 2, 3, 4, 8, 9, 10, 14, 15, and 16, then the estimated results would be representative of the rigidity ratio within the second zone combination (i.e., ZC2).

The equivalent tensile stress distribution of the plate induced by the virtual force configuration applied at this set of points is shown in Fig. 13. We observed the stress to be concentrated within the ZC2; hence, according to the theoretical basis of the PLFM, the rigidity ratio of ZC2 could be estimated. In a similar manner, by applying the virtual force configuration at different sets of points, the rigidity ratio within all 12 ZCs could be estimated. The corresponding displacements $\boldsymbol{x}^1$ for each of the measured DOFs could be calculated with (18) by using the truncated flexibility matrices constructed with a different number of modes and f^1.

Fig. 14 shows the estimated rigidity ratio, *R*, when the elastic modulus of Zone 8 was reduced to 10%, 25%, 50%, 75%, and 90% using the first 10 modes. The ZCs of ZC2, ZC3, ZC6, and ZC7 were identified clearly as damaged regions with the estimated *R* by using the PLFM with lateral DOF mode shapes. The estimated reduction of the rigidity ratios in these ZCs was smaller than the value estimated using the rotational DOFs. Because only Zone 8 sustained damage, this result was deemed reasonable since the

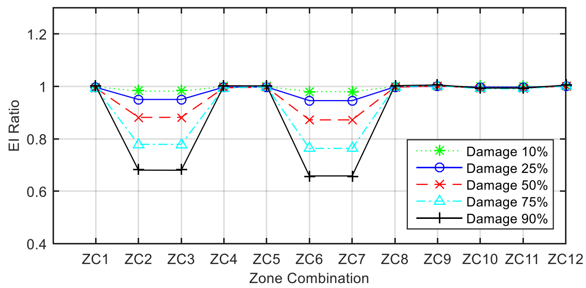

Fig. 14 The rigidity ratio of the plate structure estimated using the first 10 modes when the elastic modulus of Zone 8 was reduced to 10%, 25%, 50%, 75%, and 90% using lateral DOF mode shapes

estimated rigidity ratios were actually lump values of one and four zones when using the rotational DOFs and lateral DOFs, respectively.

Accordingly, the results of damage localization obtained using the lateral DOFs are somewhat confusing. Based on the results, one possible extreme condition was that all the zones belonging to the four ZCs (i.e., Zones 2, 3, 4, 7, 8, 9, 12, 13, and 14) suffered a similar extent of damage. The other extreme condition was that only the intersection (i.e., Zone 8) incurred damage, and to a greater extent. Moreover, any condition that comprised a linear combination of these two extreme conditions also provided a potential explanation. Nevertheless, the results of the rigidity ratios yielded useful information pertaining to the approximate locations and the extent of possible damage.

Fig. 15 shows the estimated rigidity ratio, *R*, when the elastic modulus of the six zones was reduced to 50% using the first one, three, five, seven, and ten modes. For example, regarding the results shown in Fig. 15(d), the elastic modulus of Zone 6 was reduced to 50%. The results indicated that the EI ratio was reduced at both ZC1 and ZC5. This is because the damaged Zone 6 was located within their ZCs with concentrated stress only when the force configuration was applied at ZC1 and ZC5. Fig. 15 thus shows improvements in the results when an increasing number of modes was used.

As mentioned, even the results obtained using only the first mode had already indicated the damage location clearly, and the estimated extent of damage in the damaged zone was quite close to that found using the first 10 modes. However, unlike the results obtained using the rotational DOFs, the estimated rigidity ratios of the zones adjacent to the damaged zones remained unaffected. This could be due to the greater concentration of stress induced by the virtual force configuration compared to that induced by the moment.

When both Zones 1 and 8 were damaged with a 50% reduction in elastic modulus, we obtained the results with the first 10 modes (Fig. 16). ZC1, ZC2, ZC3, ZC6, and ZC7 were identified clearly as the damaged regions, even when only the first mode was used. Again, the fact that multiple damage locations existed did not influence the damage detection results seriously. However, as discussed for the first damage scenario, many potential damage parameter combinations could lead to the same results, which

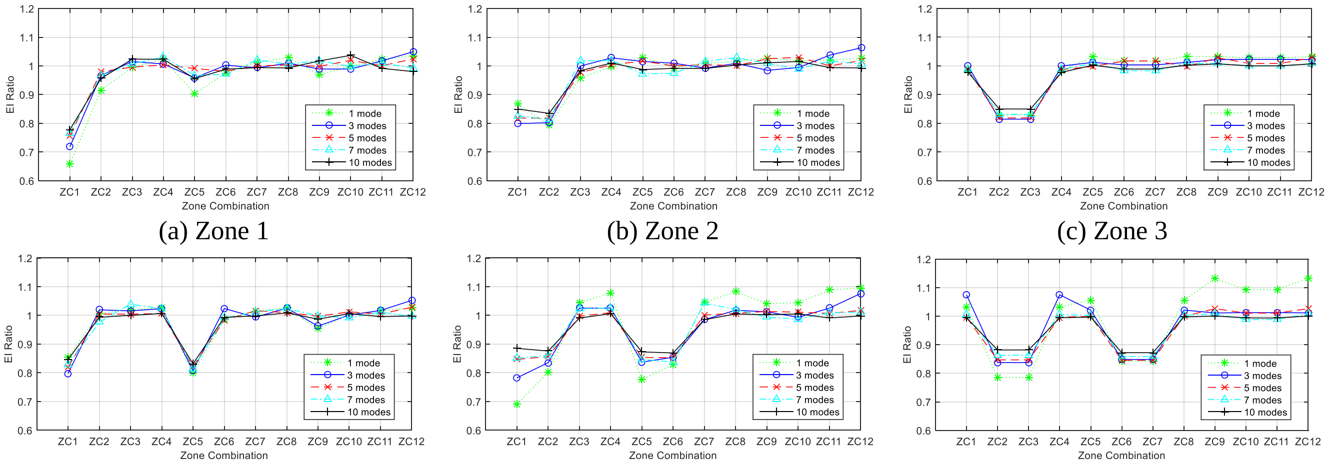

(a) Zone 1 (b) Zone 2 (c) Zone 3

(d) Zone 6 (e) Zone 7 (f) Zone 8

Fig. 15 Rigidity ratio estimated using the first one, three, five, seven, and ten modes when the elastic modulus of (a) Zone 1; (b) Zone 2; (c) Zone 3; (d) Zone 6; (e) Zone 7; and (f) Zone 8 was reduced to 50% using lateral DOF mode shapes

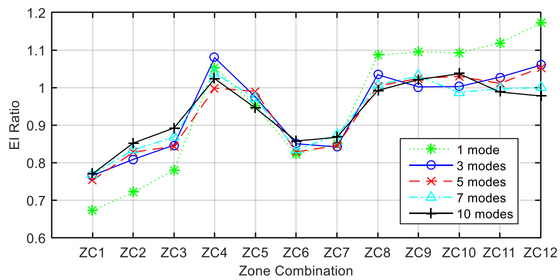

Fig. 16 Estimated rigidity ratio when both Zones 1 and 8 were damaged with a 50% reduction in elastic modulus using the lateral DOF of mode shapes

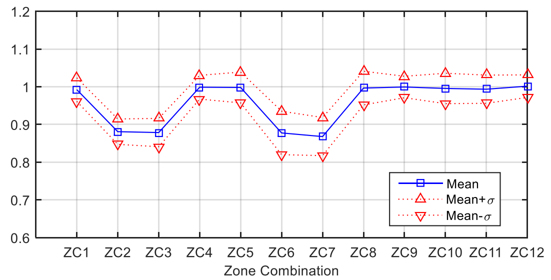

Fig. 17 Estimated rigidity ratio with 2% random noise in modal parameters when the elastic modulus of Zone 8 was reduced by 50% using the lateral DOF of mode shapes

complicates the data even further. Nevertheless, the resulting rigidity ratios provided useful information regarding the approximate locations and the extent of possible damage.

In the final scenario, both the modal frequencies and the mode shapes were contaminated with 2% random noise within one standard deviation. The damage results obtained using the first 10 modes when the elastic modulus of Zone 8 was reduced by 50% are shown in Fig. 17. We again conducted 100 trials, and we calculated the mean value as well as the mean value plus or minus one standard deviation of the rigidity ratios. The maximum and minimum of the standard deviation of all the estimated rigidity ratios in the different zones were 5.72% and 2.83%, respectively. A moderate standard deviation was achieved compared to the estimated reduction in rigidity ratio, which was approximately 12%.

4. Conclusions

This study proposed a PLFM to localize and quantify damage to a thin-plate structure. The damage detection equation, which can be used to estimate the lump flexural rigidity ratio of a local region of a thin plate, was devised based on isotropic quasistatic Kirchhoff-Love plate theory. In addition to the conventional measurement of lateral DOFs, we considered the measurement of rotational DOFs. Only the modal parameters of both the intact and damaged plate structures are necessary for the damage detection equation to estimate the flexural rigidity ratios if the mass of the plate structures can be simplified into a uniform distribution, and if the mass matrices can be simplified diagonally.

By using reasonable virtual force configurations that generate concentrated stress fields in a plate structure, a complete set of local flexural rigidity ratios for the entire plate can be calculated. Because the stress induced by the virtual force configuration is not strictly limited to the region enclosed by the virtual forces, the estimated flexural rigidity ratios are typically smaller than their real counterparts. A notable feature of the proposed method is that very few—or even just one of the lowest modes of the plate structures—can provide a reliable estimation of damage, as supported by the numerical results. Additional modes may be required to estimate the extent of damage if the proposed method is applied to different types of plates.

According to the numerical results, compared to the conventional lateral DOF measurements, the rotational DOF measurements seem to present a number of advantages and disadvantages. Because the region of the concentrated stress induced by the virtual force configuration of the rotational DOFs is much smaller, the damage location and extent are more easily interpretable.

Only one zone of the major rigidity ratio reduction is typically observed if the designated damage is located within a single zone when rotational DOFs are used. However, because the stress induced by the virtual force configuration of the rotational DOFs is not necessarily concentrated within the region enclosed by the virtual forces, the estimated rigidity ratios of the zones adjacent to the damaged zones were affected by the damaged zones, which is the main disadvantage of using rotational DOFs.

Another advantage of using the rotational DOFs is that, because the region occupied by the concentrated stress field can be much smaller than for lateral DOFs, the estimated rigidity ratio could be more sensitive to damage. Therefore, with the same level of noise in the identified modal parameters, the estimated rigidity ratios would be more robust against errors. Nevertheless, in this study, the proposed PLFM demonstrated that it can accomplish damage detection, localization, and quantification for plate structures, irrespective of whether lateral or rotational DOFs are used.

Acknowledgments

We would like to thank the National Center for Research on Earthquake Engineering in Taiwan for providing valuable assistance for our research. This research was supported in part by the Ministry of Science and Technology under the grant No MOST 106-2622-M-011-002-CC2.

References

Araujo Dos Santos, J.V., Mota Soares, C.M., Soares, C.A. and Maia, N.M.M. (2005), "Structural damage identification in laminated structures using FRF data", *Compos. Struct.*, **67**, 239-249.

Bayissa, W.L. and Haritos, N. (2007), "Structural damage identification in plates using spectral strain energy analysis", *J. Sound Vib*., **307**(1), 226-249.

Caicedo, J.M. (2003), "Structural health monitoring of flexible civil structures", PhD Thesis, Washington University

Cawley, P. and Adam, R.D. (1979), "The location of defects in structures from measurements of natural frequencies", *J. Strain Anal.*, **14**(2), 49-57.

Cornwell, P.J., Dobeling, S.W. and Farrar, C.R. (1999), "Application of the strain energy damage detection method to plate-like structures", *J. Sound Vib.*, **224**(2), 359-374.

Doebling, S.W., Farrar, C.R., Prime, M.B. and Shevitz, D.W. (1996), "Damage identification and health monitoring of structure and mechanical systems from changes in their vibration characteristics: A literature review", Research Report, No. LA-13070-MS, ESA-EA, Los Alamos National Laboratory, Los Alamos, N.M.

Fan, W. and Qiao, P. (2009), "A 2-D continuous wavelet transform of mode shape data for damage detection of plate structures", *Int. J. Solid. Struct.*, **46**(25-26), 4379-4395.

Fu, Y.Z., Lu, Z.R. and Liu, J.K. (2013), "Damage identification in plates using finite element model updating in time domain", *J. Sound Vib.*, **332**(26), 7018-7032.

Ge, M. and Lui, E.M. (2005), "Structural damage identification using system dynamic properties", *Comput. Struct.*, **83**(27), 2185-2196.

Giraldo, D.F. (2006), "A structural health monitoring framework for civil structures", PhD Thesis, Washington University.

Hsu, T.Y., Shiao, S.Y. and Liao, W.I. (2015), "A pseudo local flexibility algorithm for vibration-based damage detection of hyperstatic beams", *J. Struct. Control Hlth. Monit.*, **22**, 682-693.

Ng, C.T. (2015), "A two-stage approach for quantitative damage imaging in metallic plates using Lamb waves", *Earthq. Struct.*, **8**(4), 821-841.

Reynders, E. and De Roeck, G. (2010), "A local flexibility method for vibration-based damage localization and quantification", *J. Sound Vib.*, **329**(12), 2367-2383.

Salawu, O.S. (1997), "Detection of structural damage through changes in frequency: A review", *Eng. Struct.*, **19**(9), 718-723.

Timoshenko, S. and Woinowsky-Krieger, S. (1959), *Theory of plates and shells*, McGraw-Hill, New York, NY, USA.

Torkzadeh, P., Fathnejat, H. and Ghiasi, R. (2016), "Damage detection of plate-like structures using intelligent surrogate model", *Smart Struct. Syst.*, **18**(6), 1233-1250.

Zhang, Y., Wang, L., Lie, S.T. and Xiang, Z. (2013), "Damage detection in plates structures based on frequency shift surface curvature", *J. Sound Vib.*, **332**(25), 6,665-6,684.

KT